Structural and Functional Investigation of a Putative Archaeal Selenocysteine Synthase[†,‡]

Jens T. Kaiser,[§] Kirill Gromadski,[||] Michael Rother,[⊥,#] Harald Engelhardt,[+] Marina V. Rodnina,[||] and Markus C. Wahl*[,@]

Division of Chemistry and Chemical Engineering, California Institute of Technology, m/c 114-96, Pasadena, California 91125, Institut für Physikalische Biochemie, Universität Witten/Herdecke, Stockumer Strasse 10, D-58448 Witten, Germany, Lehrstuhl für Mikrobiologie, Ludwig-Maximilians-Universität, Maria-Ward-Strasse 1a, D-80638 München, Germany, Abteilung Molekulare Strukturbiologie, Max-Planck-Institut für Biochemie, Am Klopferspitz 18, D-82152 Martinsried, Germany, and Zelluläre Biochemie/Makromolekulare Röntgenkristallographie, Max-Planck-Institut für biophysikalische Chemie, Am Fassberg 11, D-37077 Göttingen, Germany

Received June 10, 2005; Revised Manuscript Received August 4, 2005

ABSTRACT: Bacterial selenocysteine synthase converts seryl-tRNA^{Sec} to selenocysteinyl-tRNA^{Sec} for selenoprotein biosynthesis. The identity of this enzyme in archaea and eukaryotes is unknown. On the basis of sequence similarity, a conserved open reading frame has been annotated as a selenocysteine synthase gene in archaeal genomes. We have determined the crystal structure of the corresponding protein from *Methanococcus jannaschii*, MJ0158. The protein was found to be dimeric with a distinctive domain arrangement and an exposed active site, built from residues of the large domain of one protomer alone. The shape of the dimer is reminiscent of a substructure of the decameric *Escherichia coli* selenocysteine synthase seen in electron microscopic projections. However, biochemical analyses demonstrated that MJ0158 lacked affinity for *E. coli* seryl-tRNA^{Sec} or *M. jannaschii* seryl-tRNA^{Sec}, and neither substrate was directly converted to selenocysteinyl-tRNA^{Sec} by MJ0158 when supplied with selenophosphate. We then tested a hypothetical *M. jannaschii O*-phosphoseryl-tRNA^{Sec} kinase and demonstrated that the enzyme converts seryl-tRNA^{Sec} to *O*-phosphoseryl-tRNA^{Sec} that could constitute an activated intermediate for selenocysteinyl-tRNA^{Sec} production. MJ0158 also failed to convert *O*-phosphoseryl-tRNA^{Sec} to selenocysteinyl-tRNA^{Sec}. In contrast, both archaeal and bacterial seryl-tRNA synthetases were able to charge both archaeal and bacterial tRNA^{Sec} with serine, and *E. coli* selenocysteine synthase converted both types of seryl-tRNA^{Sec} to selenocysteinyl-tRNA^{Sec}. These findings demonstrate that a number of factors from the selenoprotein biosynthesis machineries are cross-reactive between the bacterial and the archaeal systems but that MJ0158 either does not encode a selenocysteine synthase or requires additional factors for activity.

A group of organisms from all three lines of descent maintains intricate systems for decoding certain UGA triplets that would normally signal a translational stop with selenocysteine (Sec).[1] The machinery for the cotranslational incorporation of selenocysteine into selenoproteins has been elucidated in bacteria (*1*, *2*). In *Escherichia coli* (*eco*), tRNA^{Sec} (SelC) is charged with serine by seryl-tRNA synthetase (SerRS). The tRNA-bound serine is subsequently converted to selenocysteine by selenocysteine synthase (SelA) in a pyridoxal phosphate (PLP)-dependent reaction. SelA employs selenophosphate as the activated selenium donor, which is provided by selenophosphate synthetase (SelD). A homologue of EF-Tu, SelB, mediates the interaction of Sec-tRNA^{Sec}, the mRNA, and the ribosome to decode UGA stop codons, which are followed by a selenocysteine insertion (SECIS) element. The SECIS elements in bacteria lie within the protein coding regions immediately downstream of the UGA codon.

The corresponding processes are more complex in archaea (*3*−*6*) and eukaryotes (*7*−*11*), and additional factors that are

[†] This research was sponsored by the Deutsche Forschungsgemeinschaft (WA1126/2-2 and RO2004/7-1), the Max-Planck-Society, and fellowships from the Peter and Traudl Engelhorn-Stiftung to M.C.W., the Alfried Krupp von Bohlen und Halbach-Stiftung to M.V.R. and K.G., and the Fonds der Chemischen Industrie to M.V.R.

[‡] Coordinates of the refined structures of native and $NaBH_4$-reduced MJ0158 as well as the structure factors have been deposited in the Protein Data Bank as entries 2AEU and 2AEV, respectively.

* To whom correspondence should be addressed. Telephone: ++49-551-201-1046. Fax: ++49-551-201-1197. E-mail: mwahl@gwdg.de.

[§] California Institute of Technology.

[||] Universität Witten/Herdecke.

[⊥] Ludwig-Maximilians-Universität.

[#] Present address: Institute of Microbiology, Johann Wolfgang Goethe-Universität Frankfurt, Marie-Curie-Str. 9, D-60439 Frankfurt am Main, Germany.

[+] Max-Planck-Institut für Biochemie.

[@] Max-Planck-Institut für biophysikalische Chemie.

[1] Abbreviations: BSA, bovine serum albumin; CGL, cystathionine γ-lyase; CGS, cystathionine γ-synthase; *eco*, *Escherichia coli*; MBTH, 3-methyl-2-benzothiazolone hydrazone hydrochloride; *mja*, *Methanococcus jannaschii*; ORF, open reading frame; PLP, pyridoxal phosphate; PSTK, *O*-phosphoseryl-tRNA^{Sec} kinase; *sce*, *Saccharomyces cerevisiae*; Sec, selenocysteine; SECIS, selenocysteine insertion element; SelA, selenocysteine synthase; SelB, elongation factor SelB; SelC, tRNA^{Sec}; SelD, selenophosphate synthetase; SeMet, selenomethionine; Sep, *O*-phosphoserine; SepRS, Sep-tRNA^{Cys} synthetase; SerRS, seryl-tRNA synthetase; TLC, thin-layer chromatography.

10.1021/bi051110r CCC: $30.25 © 2005 American Chemical Society
Published on Web 09/17/2005

involved continue to be discovered. Certain components of the archaeal selenoprotein synthesizing machinery have initially been identified in the genome of *Methanococcus jannaschii* (*mja*) (*12*) [*mja*SerRS, open reading frame (ORF) *mj1077*; *mja*SelD, ORF *mj1591*; *mja*tRNA^{Sec}]. Subsequently, the product of ORF *mj0495* has been assigned as the archaeal elongation factor SelB (*4*). Furthermore, SECIS structures have been found, which are located outside of the coding regions (*3*, *5*), reminiscent of the situation in eukaryotes (*13*). Likewise, SelB from mammals (also termed EF-Sec) has now been identified (*9*, *11*). As novel eukaryotic factors, several SECIS binding proteins have been characterized (*14*−*16*), and conversion of Ser-tRNA^{Sec} to Sec-tRNA^{Sec} in eukaryotes seems to occur via a tRNA^{Sec}-bound *O*-phosphoserine (Sep) intermediate, which is generated by a specific *O*-phosphoseryl-tRNA^{Sec} kinase (PSTK) (*6*).

The molecular entities encoding archaeal and eukaryotic SelA activities are still unknown. We have therefore undertaken an investigation of an archaeal SelA candidate, the product of ORF *mj0158* from *M. jannaschii*. The protein was overexpressed in *E. coli* and characterized structurally and biochemically. In contrast to the decameric *eco*SelA, MJ0158 forms dimers. While the distinctive shape of these dimers resembles a substructure of *eco*SelA seen in electron microscopic projections, our biochemical analyses demonstrate that Sec-tRNA^{Sec} production in archaea may involve a Sep-tRNA^{Sec} intermediate but that recombinant MJ0158 alone does not harbor SelA activity.

EXPERIMENTAL PROCEDURES

Cloning, Expression, Purification, and Characterization. The predicted *mj0158* gene from *M. jannaschii* (http://www.tigr.org) was PCR-amplified from total genomic DNA and inserted into the pT7-7 expression vector by standard procedures. Restriction sites were chosen so that an expression product would be limited to the predicted MJ0158 sequence. The expression construct was verified by sequencing of the insert and of adjacent vector regions. To produce the encoded protein, *E. coli* BL21(DE3)-RIL cells (Stratagene) were transformed with the pT7-7-*mj0158* plasmid, and 100 mL of selective (100 μg/mL ampicillin and 34 μg/mL chloramphenicol) LB medium was inoculated with the crude transformation mix. After overnight incubation at 37 °C, cells were harvested by centrifugation, resuspended in fresh medium, and used to inoculate 1 L of selective LB cultures. After growth to an OD_{600} of 0.8−1.0, the cultures were induced with 1 mM IPTG and propagated for an additional 4−8 h at 37 °C. Cells were harvested by centrifugation, resuspended in buffer A [50 mM HEPES-NaOH (pH 8.0), 10 μM PLP, 2 mM EDTA, and 2 mM DTT], and stored at −70 °C.

After being thawed and after addition of one tablet per 50 mL of protease inhibitor mix (Complete with EDTA; Roche), the cells were disrupted with lysozyme and by sonication. Streptomycin sulfate (3%, w/v) was added to a 70000*g* clarified lysate and the precipitant removed by centrifugation. The supernatant was heated to 80 °C for 20 min, cooled on ice, and again cleared by centrifugation. The heat-resistant sample was loaded on a 150 mL DEAE-Sepharose FF column (Amersham-Pharmacia) in buffer A. The flow-through was adjusted to 1 M ammonium sulfate and loaded on a 75 mL Phenyl-Sepharose HP column (Amersham-Pharmacia) equilibrated with buffer A and 1 M ammonium sulfate. After being washed with the same buffer, the MJ0158-containing fraction was stepped off the column with buffer A. The sample was concentrated to ∼15 mg/mL by ultrafiltration (10 kDa cutoff membrane; Amicon) and adjusted to 250 mM sodium citrate (pH 4.0). After a second heat treatment (30 min at 90 °C), the supernatant was buffer-exchanged to crystallization buffer [10 mM HEPES-NaOH (pH 7.0), 10 μM PLP, and 2 mM DTT] with PD-10 columns (Amersham-Pharmacia) and concentrated to 13 mg/mL. Aliquots were shock-frozen in liquid nitrogen and stored at −70 °C. Approximately 3 mg of purified protein was obtained per liter of expression culture. Selenomethionine (SeMet)-derivatized protein was prepared in the same fashion with replacement of LB medium by minimal medium and the use of methionine-auxotrophic *E. coli* B834(DE3) cells (*17*).

Target fractions during purification were identified by SDS−polyacrylamide gel electrophoresis. To verify the nature and quality of the purified products, all preparations were N-terminally sequenced. Complete replacement of Met with SeMet was demonstrated by liquid chromatography−electrospray ionization single-quadrupole mass spectrometry (SCIEX API165; Perkin-Elmer). Mass spectrometric analysis was also undertaken for the native sample and for the native protein treated with 10 mM $NaBH_4$ for 15 min.

The PLP content of the MJ0158 preparation was determined by the method of Soda and co-workers (*18*). Briefly, the buffer of a purified MJ0158 sample was exchanged for 20 mM potassium phosphate (pH 7.4) via NAP-10 columns (Amersham-Pharmacia) to remove excess PLP, and the protein concentration was determined by the Bradford assay. H_2SO_4 (0.5 M) was added to a final concentration of 25 mM, and the sample was heated at 121 °C for 2 h (*19*). The cofactor was quantified by the colorimetric assay with 3-methyl-2-benzothiazolone hydrazone hydrochloride (MBTH) using standardization with commercial PLP in the same buffer.

Oligomerization of MJ0158 was investigated by analytical gel filtration chromatography on a SMART FPLC system (Amersham-Pharmacia) with a Superdex 75 PC 3.2/30 size exclusion column (2.4 mL gel bed, column dimensions of 3.2 mm × 300 mm), operated in phosphate-buffered saline (pH 7.4). Molecular weight standards were thyroglobulin (M_r = 670 000), β-amylase (M_r = 200 000), bovine γ-globulin (M_r = 158 000), bovine serum albumin (BSA, M_r = 66 000), chicken ovalbumin (M_r = 44 000), carbonic anhydrase (M_r = 29 000), equine myoglobin (M_r = 17 500), and vitamin B_{12} (M_r = 1300). The excluded volume (V_0) was determined with blue dextran (M_r ∼ 2 000 000) and the total volume of the liquid phase (V_t) with water. The apparent M_r of MJ0158 was deduced from plots of log(M_r) versus (V_e − V_0)/(V_t − V_0) (V_e is the observed elution volume).

Crystallization and Data Collection. Initial crystallization trials were conducted in the sitting drop format (2 μL of protein, 1 μL of reservoir) with incomplete factorial screens. Promising initial conditions were fine-screened by systematic variation of the pH and the precipitant concentrations and by addition of various trace substances (e.g., inorganic salts, electrostatic cross-linkers, and detergents). Crystals suitable for data collection were obtained with 500 μL of a reservoir

Table 1: Crystallographic Data

	SeMet			Bromide				
	peak	edge	remote	peak	edge	remote	native	reduced
Data Collection								
space group	$P2_12_12$			$P2_12_12$			$P2_12_12$	$P2_12_12$
unit cell								
a (Å)	58.0			58.0			58.1	58.0
b (Å)	73.1			72.3			73.1	72.7
c (Å)	82.9			82.4			82.9	82.6
wavelength (Å)	0.9796	0.9808	0.9500	0.9167	0.9183	0.9000	1.05	1.05
resolution (Å)	18.0−2.2	18.0−2.2	18.0−2.1	18.0−2.25	18.0−2.25	18.0−2.25	18.0−1.7	18.0−1.95
completeness (%)[a]	99.1 (99.8)	99.1 (99.8)	99.1 (99.8)	99.0 (99.8)	99.1 (97.7)	99.0 (99.7)	99.4 (99.2)	92.8 (86.4)
redundancy	3.2	3.2	3.0	3.3	3.4	3.4	4.9	2.7
$I/\sigma(I)$	22.1 (4.5)	22.4 (4.6)	21.0 (3.4)	21.9 (2.6)	21.5 (2.4)	21.6 (2.4)	21.0 (3.5)	21.6 (2.4)
R_{sym}[b] (%)	4.6 (21.1)	4.2 (21.4)	4.0 (29.8)	3.9 (33.3)	3.9 (34.3)	3.9 (37.0)	6.6 (32.0)	5.2 (21.1)
Phasing								
resolution (Å)	18.0−2.2	18.0−2.2	18.0−2.1	18.0−2.25	18.0−2.25	18.0−2.25		
no. of heavy atoms	3	3	3	6	6	6		
FOM[c]								
before DM[d]			0.33			0.51		
after DM			0.81			0.78		
Refinement								
resolution (Å)							18.0−1.7	18.0−2.0
no. of reflections								
total							37208	20860
completeness (%)							99.4	90.7
test set (%)							5.0	5.0
no. of protein atoms							2879	2879
no. of water oxygens							354	180
no. of PLP moieties							−	1
SO_4							10	9
R_{work}[e] (%)							20.8	22.5
R_{free}[e] (%)							25.9	27.0
rmsd								
bonds (Å)							0.010	0.008
angles (deg)							1.77	1.17
Wilson *B* (Å^2)							31.2	42.4
model *B* (Å^2)								
protein							35.2	38.1
water							48.4	40.6
SO_4							70.8	72.7
PLP							−	59.5
ϕ/ψ (%)								
preferred							99.1	98.5
generously allowed							0.3	0.9
disallowed							0.6	0.6
PDB entry							2AEU	2AEV

[a] Data for the last 0.1 Å in parentheses. [b] $R_{sym}(I) = \sum_{hkl}\sum_i[|I_i(hkl) - \langle I(hkl)\rangle|]/\sum_{hkl}\sum_i[I_i(hkl)]$, where $I_i(hkl)$ is the intensity of the *i*th measurement of *hkl* and $\langle I(hkl)\rangle$ is the average value of *hkl* for all *i* measurements. [c] FOM (figure of merit) $= [|F(hkl)_{best}|]/|F(hkl)|$; $\mathbf{F}(hkl)_{best} = \sum_\alpha[P(\alpha)\mathbf{F}_{hkl}(\alpha)]/\sum_\alpha[P(\alpha)]$. [d] DM is density modification (solvent flattening). [e] $R_{work} = \sum_{hkl}(||F_{obs}| - k|F_{calc}||)/\sum_{hkl}(|F_{obs}|)$; $R_{free} = \sum_{hkl\subset T}(||F_{obs}| - k|F_{calc}||)/\sum_{hkl\subset T}(|F_{obs}|)$, where $hkl\subset$T is the test set.

of 0.1 M citric acid/potassium phosphate buffer (pH 2.2), 0.4 M ammonium sulfate, and 20% (v/v) PEG400, and a drop composition of 2 μL of protein and 0.5 μL of reservoir. SeMet-derivatized protein and MJ0158 reduced for 15 min with 10 mM $NaBH_4$ could be crystallized under the same conditions as the untreated, native protein.

Crystals of MJ0158 appeared within 1 day and grew to final dimensions of 0.8 mm × 0.8 mm × 0.3 mm during the following week. They could be frozen in a liquid nitrogen stream (Oxford Cryosystems) after being transferred into perfluoropolyether, PFO-X125/03, and removal of the mother liquor. Prior to being frozen, native crystals could be derivatized with bromide by soaking for 1 min in mother liquor supplemented with 1 M NaBr.

Diffraction data of crystals of native MJ0158, MJ0158 reduced with $NaBH_4$, SeMet-derivatized MJ0158 (MAD), and a NaBr-soaked crystal (MAD) were collected at 100 K on beamline BW6 of DESY (Hamburg, Germany; Table 1).

Structure Solution, Model Building, and Refinement. All diffraction data were processed with the hkl package (*20*) with retention of the anomalous differences in the SeMet and bromide MAD data sets. The space group was determined to be $P2_12_12$, and unit cell parameters (Table 1) suggested one molecule per asymmetric unit (predicted solvent content of ∼40%). Initial interpretation and refinement of heavy atom positions and temperature factors, density modification by solvent flattening, and computation of electron density maps were performed with programs from the CCP4 collection (*21*). Three of the expected five selenium centers of the protein were located from anomalous difference Patterson maps of the SeMet peak wavelength data. The resulting experimental electron density allowed the manual construction of a partial polyalanine model with MAIN (http://www-bmb.ijs.si/doc/).

The SeMet phases were also used to locate six bromide positions in the bromide MAD data set by anomalous

difference Fourier analysis. Experimental phases from the SeMet and bromide MAD data and model phases from the partially built structures were combined with SHARP (*22*). Repeated rounds of phase combination, manual model building, and refinement allowed the sequential assembly of the molecular structure, including side chains. After a model was built with the 2.1 Å SeMet data, it could be transferred to the native (1.7 Å) and $NaBH_4$-reduced (2.0 Å) data sets.

CNS (*23*) was used for refinement, which included rounds of simulated annealing and positional and *B*-factor optimization. Subsequent refinement and model building cycles included placement of water oxygens into vacant peaks of $F_o - F_c$ difference maps. Ten intense peaks in both structures with tetrahedrally arranged lobes were modeled as sulfate ions. In addition, a unique electron density feature appeared in the neighborhood of K208 in the reduced structure. This density could be ascribed to a PLP moiety in a Schiff base linkage to the latter residue based on difference Fourier maps ($F_{reduced} - F_{native}$) using phases derived from the refined native model. The PLP phosphate group replaced one of the previously built sulfate ions. For both structures, the global anisotropic *B*-factor corrections for the two MJ0158 domains were included during the final rounds of refinement using REFMAC5 (*21*). All refinement steps worked with the entire sets of observed reflections (no intensity cutoff), and free *R*-factors (~5% of the observed reflections) were continuously monitored (Table 1).

Database Deposition. Coordinates of the refined structures of native and $NaBH_4$-reduced MJ0158 as well as the structure factors have been deposited in the Protein Data Bank as entries 2AEU and 2AEV, respectively, and will be released upon publication.

Source of Other Proteins and RNAs. If not otherwise indicated, expression vectors and cell strains were kind gifts of A. Böck (LMU München, Munich, Germany). The gene for *mja*SerRS (ORF *mj1077*) was subcloned from a pT7-7-*mj1077* expression vector into pET22b(+). The protein was expressed as described above for MJ0158 with induction at later time points ($OD_{600} \sim 2.5$). The soluble fraction of a cell lysate was heated to 90 °C for 30 min; the heat-resistant fraction was passed over DEAE-Sepharose FF and hydroxylapatite (Bio-Rad) columns, and the target fractions were identified by SDS gel electrophoresis. The purified *mja*SerRS was concentrated by ultrafiltration (30 kDa cutoff membrane; Amicon) and buffer-exchanged via a PD-10 column to 10 mM HEPES-NaOH (pH 7.0), 200 mM NaCl, and 2 mM DTT. Aliquots were shock-frozen in liquid nitrogen and stored at −70 °C.

The gene for the putative *mja*PSTK (ORF *mj1538*) was PCR-amplified from total *M. jannaschii* genomic DNA and cloned under the control of a T7 RNA polymerase promoter in the pETM11 vector (EMBL, Heidelberg, Germany) using standard procedures. The protein was expressed as described above for MJ0158 and included an N-terminal His_6 tag. It was purified by affinity chromatography of the S100 fraction of the cell lysate over a Ni−NTA column (Qiagen). Affinity-purified protein was concentrated by ultrafiltration (10 kDa cutoff membrane; Amicon) and buffer-exchanged via a PD-10 column to 10 mM HEPES-NaOH (pH 7.0), 100 mM NaCl, and 2 mM DTT. Aliquots were shock-frozen in liquid nitrogen and stored at −70 °C.

Purified *eco*SerRS was a kind gift of A. Böck. *eco*SelA, *eco*SelD, and *eco*$tRNA^{Sec}$ were prepared as described previously (*24*). *mja*$tRNA^{Sec}$ was prepared recombinantly in *E. coli* according to the method of ref *4*. It is expected to exhibit standard tRNA modifications as opposed to a bare in vitro transcript. However, these modifications may differ from those found in native *mja*$tRNA^{Sec}$.

eco$tRNA^{Sec}$ and *mja*$tRNA^{Sec}$ were aminoacylated with serine using the respective SerRS as described in ref *24*. For negative controls in activity assays (see below), we employed the PLP-dependent enzymes cystathionine γ-lyase from *Saccharomyces cerevisiae* (*sce*CGL) and cystathionine γ-synthase from *E. coli* (*eco*CGS) that were purified as described previously (refs *25* and *26*, respectively).

Filter Binding Assay. The experiments were conducted essentially as described previously for *mja*SelB (*4*). Briefly, 30 pmol of $tRNA^{Sec}$ (*eco* or *mja*) charged with [^{14}C]serine was incubated for 30 min at 37 °C with varying amounts of protein in 250 μL volumes. The samples were subsequently passed through a nitrocellulose filter and washed with 5 mL of buffer lacking protein and tRNA.

Different MJ0158 preparations were tested for binding to Ser-$tRNA^{Sec}$: MJ0158 purified as described above, MJ0158 purified with omission of the heat treatment, and S100 extracts of a MJ0158 expression culture with and without heat treatment. Tests with *eco*SelA and *eco*Ser-$tRNA^{Sec}$ constituted a positive control. In negative control experiments, MJ0158 was replaced with BSA (Sigma) or S100 extracts of "mock" expression cultures, in which *mja*SerRS had been expressed from the same vector and under the same conditions as MJ0158.

Assay for the Conversion of Ser-tRNA^{Sec} to Sec-tRNA^{Sec}. The conversion of Ser-$tRNA^{Sec}$ to Sec-$tRNA^{Sec}$ was tested as described previously (*24*). Briefly, 10 μM [^{14}C]serine-labeled Ser-$tRNA^{Sec}$ (*mja* or *eco*) was incubated in HMK buffer with 10 μM *eco*SelD, 5 mM ATP, 1 mM DTT, 250 μM sodium selenite, and 5 μM test enzyme in 30 μL volumes for 30 min at 37 °C. Setups with *eco*SelA constituted a positive control. For negative controls, we employed *sce*CGL and *eco*CGS. The reactions were stopped by the addition of $^1/_{10}$ volume of 100 mM DTT and $^1/_{10}$ volume of 1 M KOAc (pH 4.5). tRNAs were extracted from the mixtures with phenol saturated with 100 mM sodium acetate (pH 4.6), followed by precipitation by addition of 1 volume of ice-cold 2-propanol and incubation at −20 °C for 1 h. The precipitate was collected at 6000*g* for 60 min at 4 °C. The pellet was washed with 80% ethanol containing 10 mM DTT, dried under nitrogen, and resuspended in 10 μL of deacylation buffer [0.2 M ammonium carbonate (pH 8.9), 2 mg/mL $NaBH_4$, and 10 mM unlabeled seleno-DL-cystine] for 45 min at 45 °C. The hydrolysate was dried in a Speedvac, dissolved in 4 μL of water, spotted on TLC plates (Kieselgel-60), and developed in 70% ethanol for 90 min. The plates were dried and autoradiographed on X-ray film (Kodak) overnight.

Assay for the Conversion of Sep-tRNA^{Sec} to Sec-tRNA^{Sec}. For testing the conversion of Ser-$tRNA^{Sec}$ to Sep-$tRNA^{Sec}$ by the putative *mja*PSTK, the putative kinase (3.5 μM) was incubated in HMK buffer with *mja*Ser-$tRNA^{Sec}$ (10 μM), *eco*SelD (10 μM), ATP (5 mM), DTT (1 mM), and sodium selenite (250 μM) in 30 μL volumes for 30 min at 37 °C. For testing the conversion of Sep-$tRNA^{Sec}$ to Sec-$tRNA^{Sec}$ by MJ0158, 5 μM MJ0158 was added in addition to the

setup. Reactions were stopped as before and the mixtures extracted with phenol and sodium acetate (pH 4.6). The extracted tRNAs were split in half and precipitated with 2-propanol. The first halves were deacylated as before, and the liberated amino acids were analyzed on TLC plates as described above.

To verify that modification of Ser-tRNA^{Sec} by the putative *mja*PSTK constituted phosphorylation of the serine moiety, the second halves of the tRNA extracts were dissolved in 30 μL of alkaline phosphatase reaction buffer that contained 5 units of calf intestine alkaline phosphatase (Fermentas) and incubated for 30 min at 37 °C. The reaction mixtures were again phenol-extracted, precipitated, and deacylated as before. The liberated amino acids were analyzed on TLC plates as described above.

RESULTS

Phylogenetic Comparisons. The sequence of the predicted protein product of ORF *mj0158* is similar to those of bacterial SelA enzymes, particularly in the regions encompassing the presumed active sites (Figure 1A). The genomes of several archaea in addition to that of *M. jannaschii* have been sequenced, e.g., of *Methanobacterium thermoautotrophicum* (*27*), *Methanopyrus kandleri* (*28*), and *Methanococcus maripaludis* (*29*). *Mp. kandleri* and *M. maripaludis* were expected to produce selenoproteins because genes encoding SelB, SelD, and tRNA^{Sec} could be found. This expectation could be experimentally verified for *M. maripaludis* (*5*). Both organisms maintain an ORF homologous to *mj0158* (*mk0620* and *mmp0002*, respectively; Figure 1A). This conservation of MJ0158 in selenoproteinogenic archaea is consistent with its putative SelA function.

However, while it does not seem to produce selenoproteins, *Mb. thermoautotrophicum* also harbors an ORF that is highly homologous to *mj0158* (*mth1914*) (Figure 1A), arguing against a SelA activity associated with this protein. It is also possible that ORF *mth1914* constitutes a cryptic gene (*30*, *31*) or that it encodes another PLP-dependent activity.

Characterization of the Solution State and the Cofactor. To elucidate whether ORF *mj0158* encodes an archaeal SelA, we initiated structural and biochemical studies on the recombinantly expressed protein product, MJ0158. ORF *mj0158* from *M. jannaschii* could be expressed in *E. coli* under control of a T7 RNA polymerase promoter. The purified protein migrated with an apparent M_r of approximately 42 000 on SDS gels (not shown). However, analytical gel filtration analysis indicated an M_r of approximately 90 000 for MJ0158 (data not shown), suggesting that the protein forms dimers in solution. *eco*SelA, in contrast, forms decamers (*32*, *33*).

Solutions of purified MJ0158 had an intense yellow color and displayed an absorption maximum at 418 nm with an intensity that was approximately one-third of that of its 280 nm band as well as a minor maximum at 327 nm (not shown). The 418 and 327 nm absorption maxima are consistent with the aldimine and ketimine forms, respectively, of a lysine-bound PLP cofactor. The native protein was reduced with $NaBH_4$ to trap the expected PLP−lysine Schiff base linkage and subjected to mass spectrometry. While the mass of the untreated protein (41 886) was close to that calculated from the predicted sequence (41 880), the reduced fraction showed a mass increase (228) for which a covalently bound PLP moiety could well account (expected difference, 227). Finally, we analyzed the amount of PLP bound per enzyme molecule using the same strategy that was employed for *E. coli* SelA (*19*). PLP was released from MJ0158 by heating in acidic solution, and the liberated PLP was detected by reaction with MBTH (*18*). The results indicated an almost equimolar ratio of 0.94 ± 0.02 PLP moieties per protein molecule (standard deviation from three independent measurements). We concluded that *mj0158* encodes a PLP-dependent enzyme bearing one PLP cofactor per protein molecule.

Apart from SelA enzymes, limited sequence similarities of the MJ0158 homologues to enzymes involved in the metabolism of sulfur-containing amino acids can also be discerned (not shown). We tested whether MJ0158 reacted with one of the 20 common proteinogenic amino acids. The 418 nm absorption line of MJ0158 did not shift upon incubation with any of these amino acids alone. In addition, we were unable to detect cystathionine β/γ-synthase or -lyase activities in MJ0158 (data not shown). Therefore, MJ0158 does not seem to react directly with any of the 20 common proteinogenic amino acids and does not seem to be involved in transsulfuration reactions.

*Crystal Structure of MJ0158. eco*SelA has previously been investigated by electron microscopy after negative staining [EM (*33*)]. We were interested in the crystal structure of MJ0158 to see whether it is structurally homologous to *eco*SelA. Purified MJ0158 and MJ0158 reduced with $NaBH_4$ could be crystallized (see Experimental Procedures), and the structures were determined using the multiple anomalous diffraction (MAD) technique with SeMet- and bromide-derivatized crystals (Table 1). Both native and $NaBH_4$-reduced MJ0158 crystals contained one molecule per asymmetric unit, and the final models encompassed 352 of the expected 374 amino acid residues. Eleven N-terminal residues, the very C-terminal residue, and a loop between T332 and S342 were ill-defined or lacking in the electron densities. The backbones of all remaining residues were clearly defined in the final $2F_o - F_c$ electron density maps.

MJ0158 comprises two domains, both of which exhibit an α/β-fold (Figure 1B). Overall, there are 15 α-helices (labeled $\alpha1-\alpha15$ from the N- to C-terminus), two 3_{10}-helices ($3_{10}1$ and -2), and 10 β-strands ($\beta1-\beta10$). Domain I (small domain) is made up of the 35 N-terminal residues and of C-terminal residues 268−374. Amino acids 45−255 are interspersed to build up domain II (large domain). In the regions of residues 35−45 and 255−268, the polypeptide chain crosses between the two substructures.

The composite small domain I is made up of a layer of helices ($\alpha1$, $\alpha12-\alpha15$, and $3_{10}1$) that are packed against a three-stranded β-sheet ($\beta8-\beta10$) (Figure 1B). The surface of the β-sheet distal to the α-helices is exposed to the solvent. Preceding strand $\beta10$, the protein chain traverses the disordered loop, T332−S342.

The large domain II contains a central seven-stranded β-sheet (Figure 1B; $\beta1-\beta7-\beta6-\beta5-\beta4-\beta2-\beta3$ strand arrangement). All strands except $\beta7$ run in parallel. $\beta1$ and $\beta4$ of the sheet additionally engage in short β-type pairings with other regions of the domain and thus stabilize its compact structure. The concave side of the sheet is occupied by three α-helices ($\alpha4$, $\alpha5$, and $\alpha9$), whose axes are approximately parallel to the direction of the strands (Figure

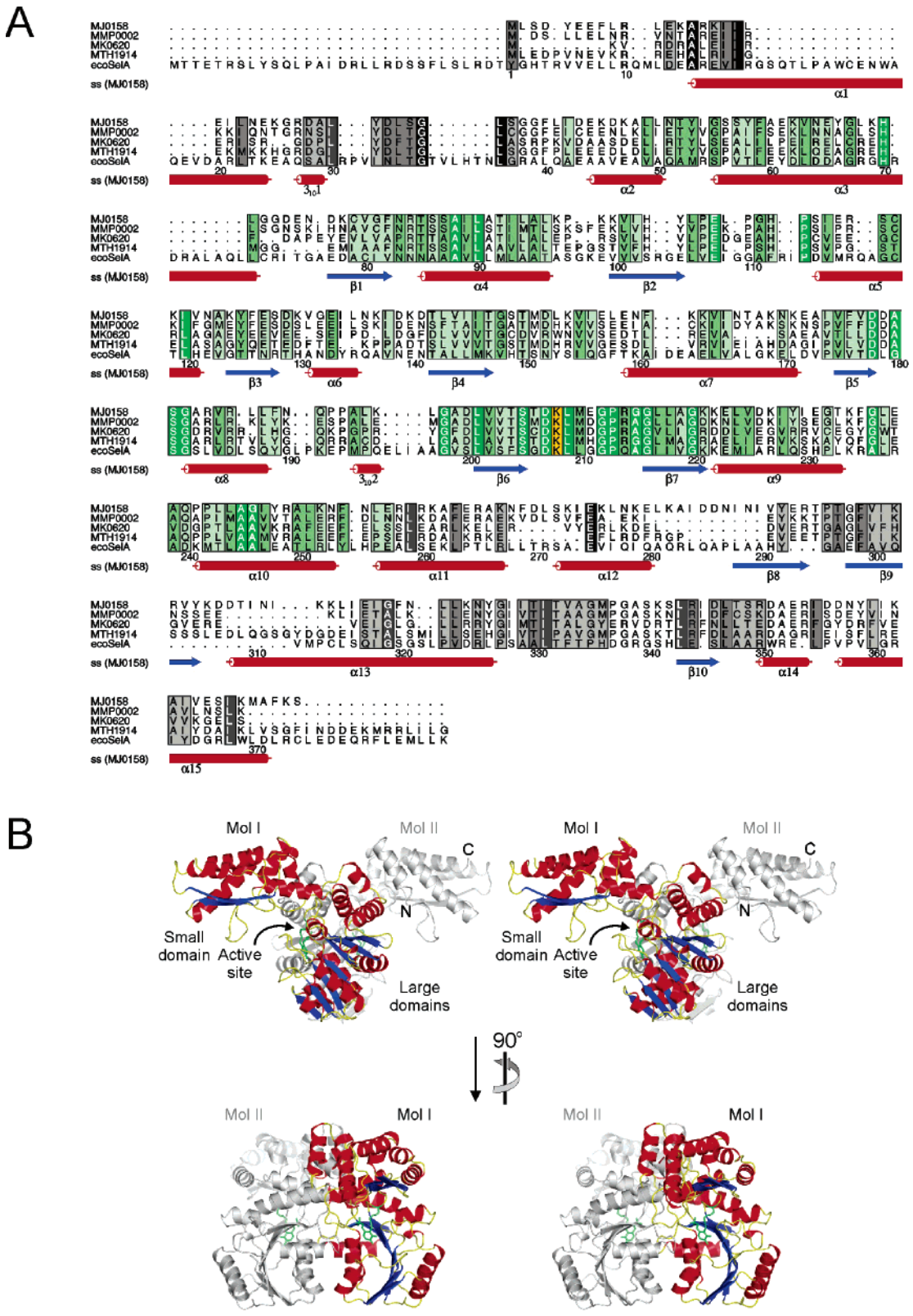

FIGURE 1: (A) Sequence alignment of MJ0158, archaeal homologues, and *eco*SelA. MMP0002 represents the product of *M. maripaludis* ORF *mmp0002*, MK0620 the product of *Mp. kandleri* ORF *mk0620*, and MTH1914 the product of *Mb. thermoautotrophicum* ORF *mth1914*. The numbering below the alignment is according to the MJ0158 sequence omitting gaps. Secondary structure elements as found in the MJ0158 structure are indicated below the alignment [ss (MJ0158)]. Sequence conservation is depicted by color-coding; a darker background corresponds to a higher degree of conservation. Conservation of residues in the small domain is depicted by different shades of gray. Conservation of residues in the large domain is depicted by different shades of green. The active site lysine (K208 in MJ0158) is highlighted in yellow. (B) Stereo ribbon plots of the MJ0158 dimer. The top panel is a front view and the bottom panel a side view. The relative viewpoints are indicated by the rotation symbol. The secondary structure elements in one monomer (Mol I) are color-coded (red for α-helices, blue for *β*-strands, and yellow for coiled regions), and the other molecule (Mol II) is colored gray. Residue K208 and the attached PLP cofactor as seen in the structure of $NaBH_4$-reduced MJ0158 are displayed as green sticks in the active sites (arrows). All structure figures were produced with PyMol (http://pymol.sourceforge.net/).

1B). Several unstructured and helical regions (α3, α6−α8, α10, and $3_{10}2$) cover the convex side of the sheet. The N-terminal connection between the two domains is made up of an extended unstructured stretch and a short helical segment (α2). The C-terminal bridge is an α-helix (α11) with the neighboring loops.

The two domains of MJ0158 are topologically similar to the two domains of NifS (*34*, *35*) and C-DES (*36*) proteins. The structure of MJ0158 therefore pertains to the α-family of PLP-dependent enzymes (*37*). The loop corresponding to T332−S342 is similarly disordered in NifS (*35*) and has been implicated in the substrate binding of this enzyme (*38*).

Quaternary Structure and Global Shape. In the crystals, two MJ0158 molecules are intimately associated with each other and are related by a crystallographic 2-fold axis (Figures 1B and 2A,B). This dimerization seen in the crystals is consistent with the formation of dimers in solution as detected by analytical gel filtration (see above). Upon association, the monomers bury ∼4400 Å^2 of combined surface area. The global arrangement of the molecules is similar to that seen for NifS and C-DES dimers. In contrast to NifS and C-DES, the MJ0158 dimers are maintained almost exclusively by contacts between the large domains. The structure confirms that MJ0158 is dimeric and does not form decamers like bacterial SelA in vitro.

Due to a significantly different relative arrangement of the two domains in MJ0158 compared to that in NifS or C-DES, the MJ0158 dimers possess a unique global shape (Figure 2B; since the global shape of NifS is quite similar to that of C-DES, only NIFS is shown in the comparison). Viewed from the front (Figure 2B, left), the MJ0158 dimer structure resembles the letter T. The small domains are spread out in opposite directions from a central stalk formed by the large domains. NifS or C-DES dimers viewed from the same direction appear to be more globular (Figure 2B, right) because their small domains fold down onto the large domains. The overall shape of the dimeric MJ0158 structure is reminiscent of the two-lobed, 5-fold repeat pattern seen in the EM projections of *eco*SelA (*33*) (Figure 2C).

Active Site Design. From sequence alignments, K208 of MJ0158 was predicted to bear the PLP cofactor (Figures 1A). The residue is situated in a crevice between the small and large domains (Figures 1B, 2A, and 3A). The native protein structure did not reveal electron density corresponding to a PLP cofactor at this position (Figure 3B). It is likely that the enzyme lost the cofactor upon prolonged incubation at acidic pH during crystallization (see Experimental Procedures). We thus attempted to trap the cofactor by reducing its expected Schiff base linkage with $NaBH_4$ and crystallized the reduced protein. As expected, a difference Fourier map ($F_{reduced} - F_{native}$) calculated with the phases derived from the refined native model clearly revealed density for the PLP pyridine ring system above the 3σ level (Figure 3C) and allowed unambiguous placement of the PLP moiety in the structure of the $NaBH_4$-reduced protein, consistent with the mass spectrometric analysis (see above). Therefore, the K208 region corresponds to the active site of MJ0158.

Decisively different from those of other PLP-dependent enzymes of the α-family, the active site environment of MJ0158 is solely composed of residues from one protomer of the dimer (Figure 3A). In addition, only residues from the large domain contribute to the active center region (Figure 3A). The pyridine ring of the PLP moiety is sandwiched between Thr85 and His111 (Figure 3A,C), similar to the situation in NifS (*34*, *35*). The PLP phosphate group is oriented toward the N-terminus of helix α4 in favorable interaction with the helix dipole moment (Figure 3C). It is furthermore anchored by a number of hydrogen bonds and salt bridges (not shown).

While other PLP-dependent enzymes tend to largely shield their cofactors from the aqueous environment and allow access of substrate molecules through rather narrow channels (*39*), the positioning of the small domains relative to the large domains in MJ0158 leads to the partial exposure of the PLP ring moiety (Figures 1B and 2A). Confinement of the active site to the monomer further augments the exposure of the cofactor (Figure 3A). These characteristics lead to a more open design of the MJ0158 active site compared to other PLP-dependent enzymes of known structure. We note that the active site design of MJ0158 seems, a priori, to be suited to yielding access to a large substrate molecule, which upon binding may exclude solvent from the reaction environment. However, some restriction on the accessibility of the active site may be exerted by the flexible loop between T332 and S342, which could not be unequivocally assigned in the electron densities.

Surface Properties and Anion Binding. Mapping the electrostatic potential at the surface of MJ0158 reveals extended positively charged regions (Figure 2A). Ten sulfate ions could be identified in the apoenzyme structure (Figure 3B) and nine in the holoenzyme structure, where one sulfate is replaced with the PLP phosphate group (Figure 3C). Both sulfate and phosphate ions are present in the crystallization buffer, but their distinction by crystallographic means is not possible at the present resolutions. Because of their higher concentration in the mother liquor, we have modeled sulfate ions. Two complex anions were found within the active site region on either side of the His111 side chain (Figure 3). One of them ($SO_4$1 in Figure 3) is also found in a similar position, e.g., in the *Thermotoga maritima* NifS structure (*35*). The other anion in the active site is unique to MJ0158 ($SO_4$2 in Figure 3). For other PLP-dependent enzymes, it has been suggested that such anions mimic negatively charged groups, such as a carboxylate function, on the substrate molecule (*39*).

On the basis of the structural analysis alone, we could not decide whether MJ0158 harbors SelA activity. We therefore investigated this question directly by conducting a series of biochemical assays.

MJ0158 Fails To Bind to Ser-tRNA^{Sec}. Since SelA enzymes bind Ser-tRNA^{Sec} (*32*), we used a nitrocellulose filter binding assay to test whether MJ0158 binds to Ser-tRNA^{Sec} from *E. coli*. Previously, it has been shown that heterologous bacterial and eukaryotic tRNA^{Sec} can complement to some degree the selenocysteine decoding machinery of *E. coli* (*40*). Therefore, we expected an archaeal SelA likewise to show some affinity for *eco*Ser-tRNA^{Sec}. Compared to *eco*SelA, MJ0158 retained *eco*Ser-tRNA^{Sec} only weakly on nitrocellulose filters, like completely unrelated proteins (not shown).

Because it is possible that MJ0158 requires specific sequences of *mja*tRNA^{Sec} for a strong interaction, we also tested its interaction with *mja*Ser-tRNA^{Sec}. The tRNA was overproduced in *E. coli* as described previously (*4*) and charged with [^{14}C]serine using recombinantly produced *mja*SerRS. This enzyme also efficiently charged tRNA^{Sec} from *E. coli*, corroborating our assumption of some cross

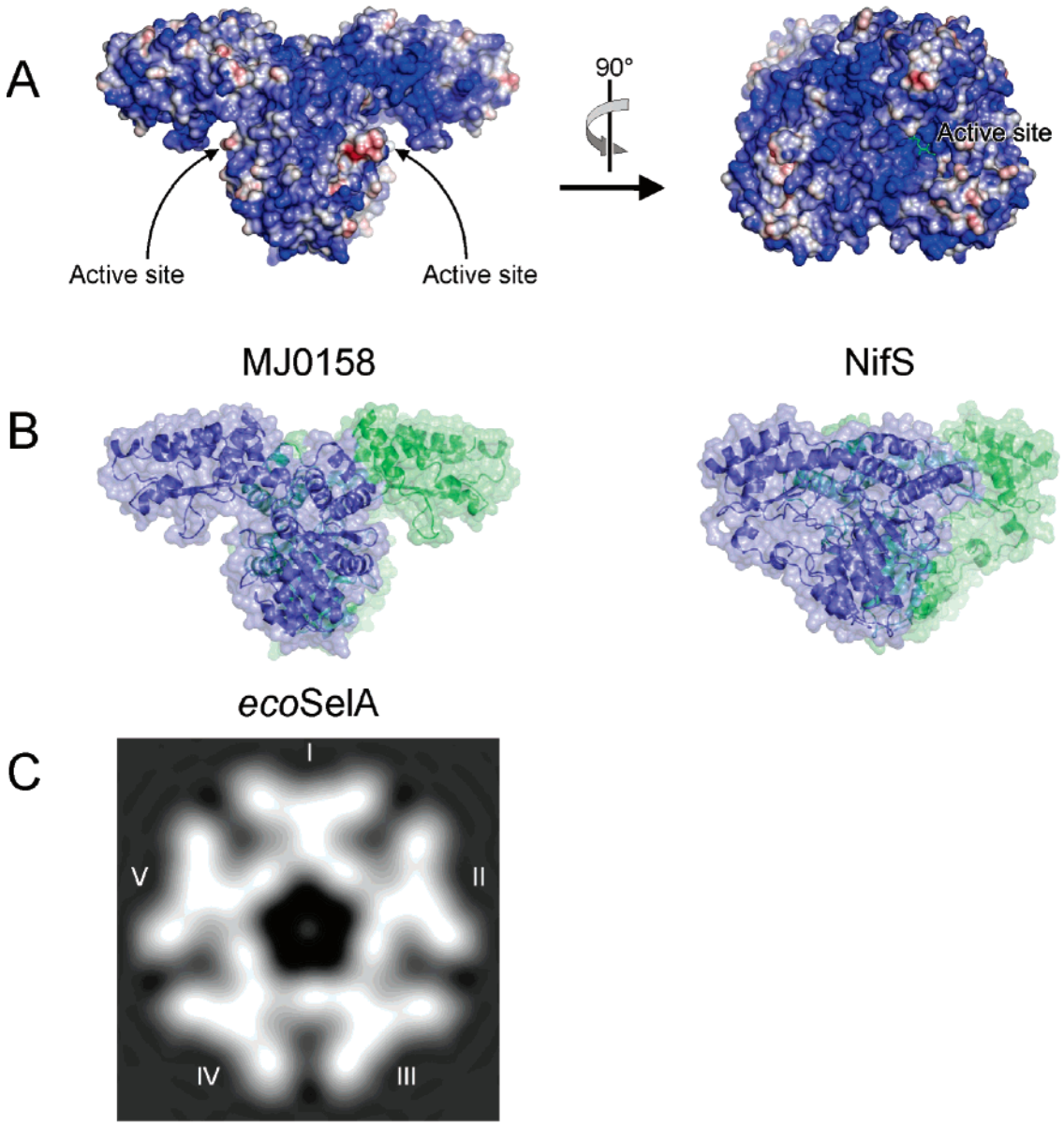

FIGURE 2: Shape and surface properties. (A) Two orthogonal views of the electrostatic surface potential of the MJ0158 dimer. Blue indicates positive charge, and red indicates negative charge. At the left is the front view and at the right a side view. The orientations of the panels are the same as in Figure 1B. The active sites are labeled. The electrostatic potential was calculated with the program APBS (https://gridport.npaci.edi/apbs/). (B) Comparison of the van der Waals surfaces of the MJ0158 dimer (left) and the *T. maritima* NifS dimer (right) in the same orientation after superpositioning of the large domains. The view is the same as in the top part of Figure 1B. Ribbon plots of the molecules are shown through the semitransparent surfaces. The protomers of the dimers are colored blue and green. The comparison reveals the significantly different shapes of the two complexes. (C) Negative-stain electron microscopic projection image of *eco*SelA (determined in ref *33*). Five repeating substructures that bear two lobes at the outside are labeled I−V. These substructures apparently correspond to the MJ0158 dimer.

reactivity between the bacterial and archeal systems (not shown). Like the interaction studies with *eco*Ser-tRNA^{Sec}, nitrocellulose filter binding studies failed to detect a significant interaction between MJ0158 and *mja*Ser-tRNA^{Sec} (Figure 4A). This result did not change when we omitted heating of MJ0158 during purification or used S100 extracts from MJ0158 expression cultures instead of the purified protein (Figure 4A). In contrast, *eco*SelA efficiently bound to *mja*Ser-tRNA^{Sec} (Figure 4A), again confirming the compatibility of some components of the bacterial and archaeal selenoprotein biosynthesis components. These results argue against a SelA function for MJ0158.

MJ0158 Does Not Directly Convert Ser-tRNA^{Sec} to Sec-tRNA^{Sec}. The nitrocellulose filters may have retained MJ0158 less efficiently than *eco*SelA, or the interaction of MJ0158 with Ser-tRNA^{Sec} may be characterized by fast binding and dissociation. We therefore tested directly whether MJ0158 can convert Ser-tRNA^{Sec} to Sec-tRNA^{Sec} when supplied with selenophosphate. SelA activity was analyzed in a coupled assay with *eco*SelD (*32*). ^{14}C-labeled *eco*Ser-tRNA^{Sec} or *mja*Ser-tRNA^{Sec} was incubated with sodium selenite, ATP, DTT, *eco*SelD, and either *eco*SelA, MJ0158, or various control proteins (BSA, *sce*CGL, and *eco*CGL). Under these conditions, *eco*SelD provides the cosubstrate selenophosphate in situ (*32*). After incubation, the tRNA fractions were extracted with phenol and deacylated, and the associated amino acids were identified by TLC (Figure 4B). Under our conditions, serine migrates above selenocysteine on the TLC

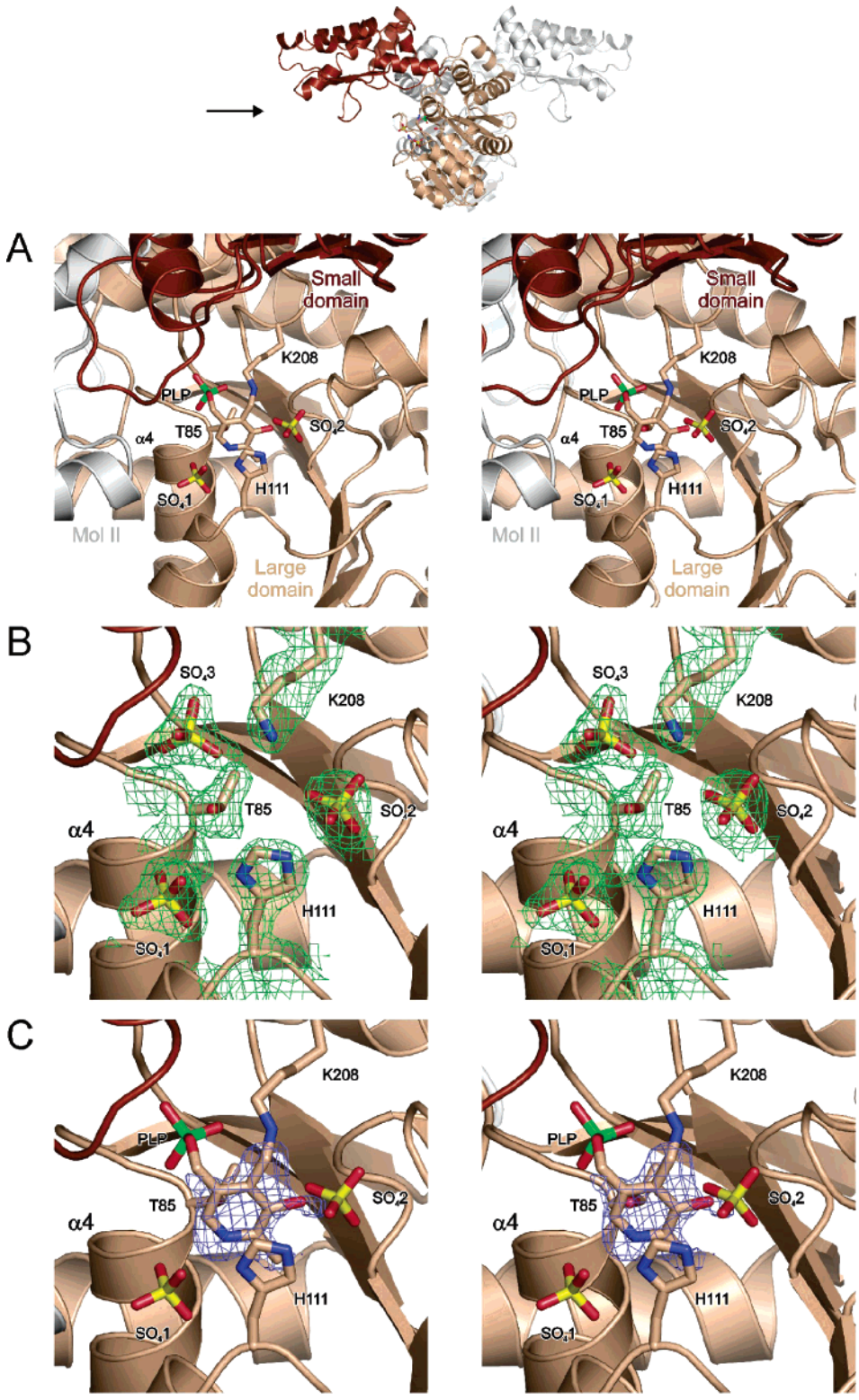

FIGURE 3: Stereo ribbon plots of the active site region of one MJ0158 protomer in the dimer with selected side chains and ligands as stick graphics. The arrow on the small icon at the top (orientation the same as in the top part of Figure 1B) indicates the viewpoint. The reference protomer is colored beige (large domain) and brown (small domain) and the other protomer light gray. (A) Active site environment. The small domain (labeled, at the top) and the other protomer (Mol II) do not participate in the buildup of the active site. K208 carries the PLP cofactor. The PLP pyridine ring stacks between the side chains of T85 and H111. Sulfate ions ($SO_4$1 and $SO_4$2) are neighboring H111 and the cofactor on either side. Atoms are color-coded by atom type: beige for carbon, blue for nitrogen, red for oxygen, yellow for sulfur, and green for phosphorus. (B) Close-up view of the active site region in native MJ0158 showing the final $2F_o - F_c$ electron density map (green mesh) covering selected elements and contoured at the 1σ level. A sulfate ion ($SO_4$3) replaces the PLP phosphate group in the apo structure. Relevant residues and ligands are labeled. Color-coding for atoms is as in panel A. (C) Close-up view of the active site region in $NaBH_4$-reduced MJ0158 showing a difference Fourier map ($F_{reduced} - F_{native}$) using phases derived from the refined native MJ0158 model (blue mesh) contoured at the 3σ level. The main differences between the apo- and holoenzyme structures defined by this map identify the position and orientation of the PLP pyridine ring. Relevant residues and ligands are labeled. Color-coding for atoms is as in panel A.

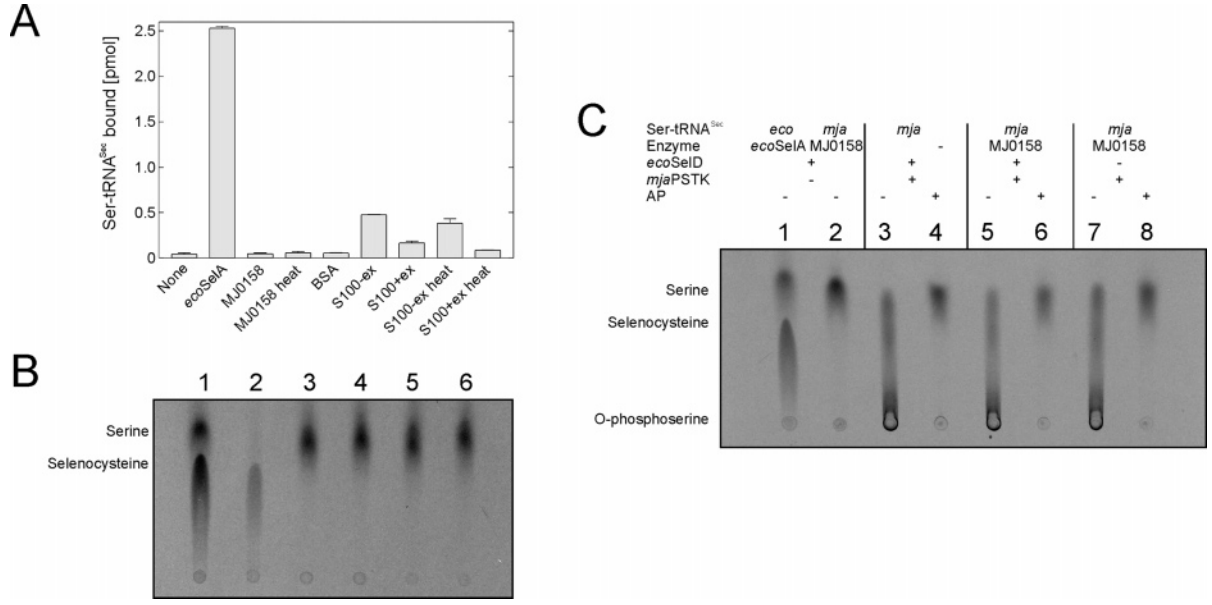

FIGURE 4: Activity tests. (A) Nitrocellulose filter binding assay for detecting the affinity of various enzyme preparations for *mja*Ser-tRNA^{Sec}. The samples that were tested are indicated below the bars: *eco*SelA, *E. coli* SelA; MJ0158, non-heat-treated MJ0158; MJ0158 heat, heat-treated MJ0158; BSA, bovine serum albumin; S100-ex, S100 extract from a mock expression culture; S100+ex, S100 extract from a MJ0158 expression culture; S100-ex heat, heat-treated S100 extract from a mock expression culture; and S100+ex heat, heat-treated S100 extract from a MJ0158 expression culture. The mock expression was an expression of *mja*SerRS in the same vector and under the same conditions as for MJ0158. This control therefore shows some heat-resistant binding to Ser-tRNA^{Sec}. (B) Assay for the direct conversion of Ser-tRNA^{Sec} to Sec-tRNA^{Sec} using *E. coli* (lane 1) or *M. jannaschii* (lanes 2−6) [^{14}C]Ser-tRNA^{Sec} as the substrate. The cosubstrate, selenophosphate, was generated in situ by the action of *eco*SelD with Na_2SO_3, DTT, and ATP (*32*). Migration positions of serine and selenocysteine on the TLC plates are indicated at the left. To obtain the migration positions of serine and selenocysteine originating from the reaction assays, reaction conditions for an incomplete conversion were used for the *E. coli* system (lane 1). The following samples were tested for SelA activity: lane 1, *eco*SelA (with *eco*Ser-tRNA^{Sec}, conditions of partial conversion); lane 2, *eco*SelA (with *mja*Ser-tRNA^{Sec}); lane 3, MJ0158; lane 4, BSA; lane 5, *sce*CGL; and lane 6, *eco*CGS. Only *eco*SelA shows the expected conversion activity irrespective of the substrate being *eco*Ser-tRNA^{Sec} (lane 1) or *mja*Ser-tRNA^{Sec} (lane 2). (C) Assay for the conversion of Ser-tRNA^{Sec} to Sec-tRNA^{Sec} via an intermediate Sep-tRNA^{Sec} using *E. coli* (lane 1) or *M. jannaschii* (lanes 2−8) [^{14}C]Ser-tRNA^{Sec} as the substrate. The cosubstrate, selenophosphate, was generated in situ by the action of *eco*SelD with Na_2SO_3, DTT, and ATP (*32*). The putative intermediate, Sep-tRNA^{Sec}, was generated by addition of *mja*PSTK. Migration positions of serine, selenocysteine, and *O*-phosphoserine on the TLC plates are indicated at the left. To obtain the migration positions of serine and selenocysteine originating from the reaction assays, reaction conditions for an incomplete conversion were used for the *E. coli* system (lane 1, no *mja*PSTK, same as lane 1 of panel B). As a negative control, a reaction setup employing MJ0158 but omitting *mja*PSTK was used in lane 2 (same as lane 3 of panel B). The following samples were tested: lane 3, *mja*PSTK alone; lane 5, MJ0158 and *mja*PSTK; and lane 7, MJ0158 and *mja*PSTK, no *eco*SelD. In reaction mixtures containing *mja*PSTK (lanes 3, 5, and 7), a new spot appeared, which essentially remained at the origin. To verify that the new spot corresponds to *O*-phosphoserine and that no selenocysteine product is hidden in the smear under the serine spot, one-half of each reaction mixture was treated with alkaline phosphatase before deacylation and applied to the TLC plate (lanes 4, 6, and 8, respectively; see Experimental Procedures for details). Upon alkaline phosphatase treatment, the spots at the origins disappeared and radioactivity was shifted to the position of serine. No hidden traces of selenocysteine were discovered.

plates (*32*). Irrespective of the source of tRNA^{Sec}, no selenocysteine was produced in reactions that included MJ0158 (lane 3), BSA (lane 4), *sce*CGL (lane 5), or *eco*CGL (lane 6). In contrast, selenocysteine was efficiently produced in the positive controls with *eco*SelA (Figure 4B, lanes 1 and 2). *eco*SelA acted on both Ser-tRNA^{Sec} from *E. coli* (Figure 4B, lane 1) and Ser-tRNA^{Sec} from *M. jannaschii* (Figure 4B, lane 2). These results demonstrate that MJ0158 alone does not harbor an activity to directly convert Ser-tRNA^{Sec} to Sec-tRNA^{Sec} using selenophosphate. We also failed to detect SelA activity in raw extracts of expression cultures of MJ0158 (not shown).

The Product of M. jannaschii ORF mj1538 Is an O-Phosphoseryl-tRNA^{Sec} Kinase. Recently, a kinase which converts Ser-tRNA^{Sec} to Sep-tRNA^{Sec} has been characterized in mammals. On the basis of these findings, it is assumed that in eukaryotes Sep-tRNA^{Sec} (as opposed to Ser-tRNA^{Sec} in bacteria) is the direct precursor to Sec-tRNA^{Sec} (*6*). An ORF encoding a protein that is homologous to this kinase can also be found in *M. jannaschii* (ORF *mj1538*) (*6*). We cloned, expressed, and purified the putative kinase as an N-terminal His_6 tag fusion protein. The recombinant enzyme converted the serine of *mja*Ser-tRNA^{Sec} to a species that migrated slower than serine or selenocysteine in TLC, consistent with the conversion of Ser-tRNA^{Sec} to Sep-tRNA^{Sec} (Figure 4C, lane 3). When the reaction mixture was treated with alkaline phosphatase before deacylation, TLC analysis revealed that the novel spot disappeared and the radioactivity was shifted into the serine position (lane 4). These results demonstrate that ORF *mj1538* indeed encodes an enzyme that acts as a PSTK in vitro and that this enzymatic activity may be involved in Sec-tRNA^{Sec} synthesis in archaea. We refer to this enzyme as *mja*PSTK.

MJ0158 Does Not Convert O-Phosphoseryl-tRNA^{Sec} to Selenocysteyl-tRNA^{Sec}. We next asked whether MJ0158 can act on Sep-tRNA^{Sec} instead of Ser-tRNA^{Sec} to produce Sec-tRNA^{Sec}. We added MJ0158 to reaction mixtures, in which selenophosphate (by the action of *eco*SelD) and Sep-tRNA^{Sec} (by the action of *mja*PSTK) were produced, and incubated the setups for 30 min at 37 °C. The product tRNAs were

extracted with phenol and deacylated. The liberated amino acids were analyzed by TLC as before (Figure 4C, lane 5). The results looked virtually identical to the results without MJ0158 (lane 3). To rule out the possibility that trace amounts of selenocysteine were hidden in the smear under the serine spot, we also treated the reaction mixture with alkaline phosphatase before deacylation. The results (lane 6) again looked identical to those without MJ0158 (lane 4) and did not reveal any trace of selenocysteine. We concluded that MJ0158 did not convert Sep-tRNA^{Sec} to Sec-tRNA^{Sec} in this assay.

DISCUSSION

The enzyme harboring SelA activity in archaea and eukaryotes is presently unknown, but ORF *mj0158* in *M. jannaschii* as well as homologous ORFs in other archaeal genomes have been assigned this function on the basis of sequence similarities to bacterial SelA enzymes (Figure 1). To test the alleged SelA function of protein MJ0158 and homologues, we conducted a combined structural and functional analysis of the enzyme.

Our crystal structures of MJ0158 before and after reduction with $NaBH_4$ revealed a dimeric PLP-containing molecule with a unique arrangement of small and large domains. The resulting shape of the dimer resembles a two-lobed substructure seen in electron microscopic projections of *eco*SelA (Figure 2C). These observations strengthen the notions that *eco*SelA is organized as a pentamer of dimers (*33*) and that the MJ0158 structure is similar to that of the dimeric substructure of *eco*SelA. At present, we are attempting to determine the three-dimensional solution structure of a bacterial SelA by cryo-EM to verify these suggestions.

The relative apposition of the two domains in MJ0158 leads to an open active site design and the lack of participation of the small domain in the formation of the active site environment. In addition, the active site is built up only from residues of one protomer of the dimer. Together, these architectural features render the active center potentially accessible to large molecules (Figures 1B and 3). In addition, MJ0158 displays a remarkably positively charged surface (Figure 2A), to which several complex anions are attached in the structures presented here. Such surface features seem to be suitable for the interaction with the negatively charged sugar−phosphate backbone of the putative substrate molecule, Ser- or Sep-tRNA^{Sec}. Therefore, several aspects of the MJ0158 structure are compatible with its putative SelA activity.

Nevertheless, other structural findings did not live up to the expectations of a SelA enzyme based on what is known about bacterial SelA. For example, the MJ0158 dimers (Figure 1B) did not associate into decamers as seen for *eco*SelA (*19*, *33*). We therefore tested directly the ability of MJ0158 to (1) interact with Ser-tRNA^{Sec}, the substrate molecule of bacterial SelA (Figure 4A), and (2) convert Ser-tRNA^{Sec} to Sec-tRNA^{Sec} in a selenophosphate-dependent manner (Figure 4B). MJ0158 exhibited neither of the expected activities. These results are not a consequence of heating the protein during purification, since nonheated extracts did not exhibit the expected activities either (Figure 4A).

Recently, it has been suggested that in eukaryotes and possibly in archaea Sec-tRNA^{Sec} synthesis requires an activated form of Ser-tRNA^{Sec}, Sep-tRNA^{Sec}, and that this precursor is generated through phosphorylation of Ser-tRNA^{Sec} by a Sep-tRNA^{Sec} kinase (*6*). Interestingly, a similar precursor molecule, Sep-tRNA^{Cys}, has just been found to be essential for the synthesis of Cys-tRNA^{Cys} in a group of methanogenic archaea that lack a recognizable Cys-tRNA^{Cys} synthetase (*41*). In this case, however, a Sep-tRNA^{Cys} synthetase (SepRS) was characterized that directly charged tRNA^{Cys} with *O*-phosphoserine (*41*). A second enzymatic activity (Sep-tRNA^{Cys}:Cys-tRNA^{Cys} synthase) was then found to be able to employ inorganic sulfide to convert Sep-tRNA^{Cys} to Cys-tRNA^{Cys} (*41*). A similar direct charging of tRNA^{Sec} with *O*-phosphoserine by SepRS was not observed, and instead, tRNA^{Sec} was charged with serine by a dialyzed S100 extract supplemented with the 20 common proteinogenic amino acids (*41*). Consistently, we were able to charge *mja*tRNA^{Sec} with serine by using *mja*SerRS (ORF *mj1077*). The product of the ORF *mj1538* indeed converted tRNA^{Sec}-bound serine to a different species that migrated consistent with *O*-phosphoserine in TLC and could be reverted to serine by alkaline phosphatase (Figure 4C). Thus, our results strengthen the notion that MJ1538 is an archaeal PSTK. Despite the provision of a better leaving group on Sep-tRNA^{Sec} (phosphate) as opposed to Ser-tRNA^{Sec} (water) for the production of the aminoacrylyl-tRNA^{Sec} intermediate for selenocysteine synthesis (*32*), MJ0158 failed to convert Sep-tRNA^{Sec} to Sec-tRNA^{Sec} (Figure 4C).

In the course of our studies, we have demonstrated that a number of factors involved in selenoprotein biosynthesis in archaea are compatible with the *E. coli* system and vice versa. For example, *mja*SerRS was able to charge *eco*tRNA^{Sec} with serine and vice versa; *eco*SelA was able to bind Ser-tRNA^{Sec} from *M. jannaschii* (Figure 4A) and to convert it to Sec-tRNA^{Sec} (Figure 4B), consistent with previous findings (*4*). The situation is perhaps different with the archaeal SelA, which may require additional factors for activity. Such unknown factors could explain why MJ0158 did not exhibit SelA activity in our assays. One upstream factor required may be the PSTK characterized herein that was not sufficient, however, for uncovering the putative SelA activity of MJ0158. We also failed to detect SelA activity in raw extracts of expression cultures of MJ0158 (not shown). Therefore, factors from the soluble *E. coli* fraction cannot substitute for the potentially required additional protein components from *M. jannaschii*.

Previous examples which document that certain components of the archaeal selenoprotein biosynthesis machinery are more complex than the corresponding factors from bacteria exist. For example, archaeal SelB (*4*) and eukaryotic SelB (*9*, *11*) are C-terminally truncated compared to bacterial SelB and have lost the ability to bind directly to mRNA SECIS elements. In eukaryotes, SECIS binding protein 2 (*42*) may act as an adaptor between SelB and the SECIS element (*9*), and a similar adaptor may exist in archaea.

In conclusion, the results presented herein demonstrate that recombinantly produced MJ0158 does not exhibit selenocysteine synthase activity in isolation. Thus, our findings question the assignment of the corresponding ORF in sequenced archaeal genomes as a selenocysteine synthase gene. A different function for the product of ORF *mj0158* would also be in better agreement with the conservation of the protein in archaea that do not seem to produce selenoproteins (Figure 1A). As an alternative, MJ0158 may require other factors beyond PSTK for activity.

ACKNOWLEDGMENT

We thank Gleb P. Bourenkov, beamline BW6 at DESY, for help during synchrotron data collection and Rasso Willkomm, Max-Planck-Institut für Biochemie, for help with cloning and purification of *mja*SerRS. We are grateful to August Böck, LMU München, for making available to us various cell strains, expression vectors, and protein preparations.

REFERENCES

1. Böck, A., Forchhammer, K., Heider, J., Leinfelder, W., Sawers, G., Veprek, B., and Zinoni, F. (1991) Selenocysteine: The 21st amino acid, *Mol. Microbiol. 5*, 515−520.
2. Stadtman, T. C. (1996) Selenocysteine, *Annu. Rev. Biochem. 65*, 83−100.
3. Wilting, R., Schorling, S., Persson, B. C., and Böck, A. (1997) Selenoprotein synthesis in archaea: Identification of an mRNA element of *Methanococcus jannaschii* probably directing selenocysteine insertion, *J. Mol. Biol. 266*, 637−641.
4. Rother, N., Wilting, R., Commans, S., and Böck, A. (2000) Identification and characterisation of the selenocysteine-specific translation factor SelB from the archaeon *Methanococcus jannaschii*, *J. Mol. Biol. 299*, 351−358.
5. Rother, M., Resch, A., Gardner, W. L., Whitman, W. B., and Böck, A. (2001) Heterologous expression of archaeal selenoprotein genes directed by the SECIS element located in the 3′ non-translated region, *Mol. Microbiol. 40*, 900−908.
6. Carlson, B. A., Xu, X. M., Kryukov, G. V., Rao, M., Berry, M. J., Gladyshev, V. N., and Hatfield, D. L. (2004) Identification and characterization of phosphoseryl-tRNA[Ser]Sec kinase, *Proc. Natl. Acad. Sci. U.S.A. 101*, 12848−12853.
7. Reddy, P. S. (1996) Biosynthesis of selenoproteins, *Curr. Sci. 71*, 735−737.
8. Low, S. C., and Berry, M. J. (1996) Knowing when not to stop: Selenocysteine incorporation in eukaryotes, *Trends Biochem. Sci. 21*, 203−208.
9. Tujebajeva, R. M., Copeland, P. R., Xu, X. M., Carlson, B. A., Harney, J. W., Driscoll, D. M., Hatfield, D. L., and Berry, M. J. (2000) Decoding apparatus for eukaryotic selenocysteine insertion, *EMBO Rep. 1*, 158−163.
10. Berry, M. J. (2000) Recoding UGA as selenocysteine, *Trans. Control Gene Expression 39*, 763−783.
11. Fagegaltier, D., Hubert, N., Yamada, K., Mizutani, T., Carbon, P., and Krol, A. (2000) Characterization of mSelB, a novel mammalian elongation factor for selenoprotein translation, *EMBO J. 19*, 4796−4805.
12. Bult, C. J., White, O., Olsen, G. J., Zhou, L., Fleischmann, R. D., Sutton, G. G., Blake, J. A., FitzGerald, L. M., Clayton, R. A., Gocayne, J. D., Kerlavage, A. R., Dougherty, B. A., Tomb, J. F., Adams, M. D., Reich, C. I., Overbeek, R., Kirkness, E. F., Weinstock, K. G., Merrick, J. M., Glodek, A., Scott, J. L., Geoghagen, N. S. M., and Venter, J. C. (1996) Complete genome sequence of the methanogenic archaeon, *Methanococcus jannaschii*, *Science 273*, 1058−1073.
13. Berry, M. J., Banu, L., Harney, J. W., and Larsen, P. R. (1993) Functional characterization of the eukaryotic SECIS elements which direct selenocysteine insertion at UGA codons, *EMBO J. 12*, 3315−3322.
14. Hubert, N., Walczak, R., Carbon, P., and Krol, A. (1996) A protein binds the selenocysteine insertion element in the 3′-UTR of mammalian selenoprotein mRNAs, *Nucleic Acids Res. 24*, 464−469.
15. Copeland, P. R., and Driscoll, D. M. (1999) Purification, redox sensitivity, and RNA binding properties of SECIS-binding protein 2, a protein involved in selenoprotein biosynthesis, *J. Biol. Chem. 274*, 25447−25454.
16. Fujiwara, T., Busch, K., Gross, H. J., and Mizutani, T. (1999) A SECIS binding protein (SBP) is distinct from selenocysteyl-tRNA protecting factor (SePF), *Biochimie 81*, 213−218.
17. Budisa, N., Steipe, B., Demange, P., Eckerskorn, C., Kellermann, J., and Huber, R. (1995) High-level biosynthetic substitution of methionine in proteins by its analogs 2-aminohexanoic acid, selenomethionine, telluromethionine and ethionine in *Escherichia coli*, *Eur. J. Biochem. 230*, 788−796.
18. Soda, K., Yorifuji, T., Misono, H., and Moriguchi, M. (1969) Spectrophotometric determination of pyridoxal and pyridoxal 5′-phosphate with 3-methyl-2-benzothiazolone hydrazone hydrochloride, and their selective assay, *Biochem. J. 114*, 629−633.
19. Forchhammer, K., Leinfelder, W., Boesmiller, K., Veprek, B., and Böck, A. (1991) Selenocysteine synthase from *Escherichia coli*. Nucleotide sequence of the gene (*selA*) and purification of the protein, *J. Biol. Chem. 266*, 6318−6323.
20. Otwinowski, Z., and Minor, W. (1996) Processing of X-ray diffraction data collected in oscillation mode, *Methods Enzymol. 276*, 307−326.
21. Collaborative Computational Project No. 4 (1994) The CCP4 Suite: Programs for protein crystallography, *Acta Crystallogr. D50*, 760−763.
22. La Fortelle, E. d., and Bricogne, G. (1997) Maximum-likelihood heavy-atom parameter refinement in the MIR and MAD methods, *Methods Enzymol. 276*, 472−494.
23. Brunger, A. T., Adams, P. D., Clore, G. M., DeLano, W. L., Gros, P., Grosse-Kunstleve, R. W., Jiang, J. S., Kuszewski, J., Nilges, M., Pannu, N. S., Read, R. J., Rice, L. M., Simonson, T., and Warren, G. L. (1998) Crystallography & NMR system: A new software suite for macromolecular structure determination, *Acta Crystallogr. D54*, 905−921.
24. Thanbichler, M., and Böck, A. (2002) Selenoprotein biosynthesis: Purification and assay of components involved in selenocysteine biosynthesis and insertion in *Escherichia coli*, *Methods Enzymol. 347*, 3−16.
25. Steegborn, C., Clausen, T., Sondermann, P., Jacob, U., Worbs, M., Marinkovic, S., Huber, R., and Wahl, M. C. (1999) Kinetics and inhibition of recombinant human cystathionine γ-lyase: Toward the rational control of transsulfuration, *J. Biol. Chem. 274*, 12675−12684.
26. Wahl, M. C., Huber, R., Prade, L., Marinkovic, S., Messerschmidt, A., and Clausen, T. (1997) Cloning, purification, crystallization, and preliminary X-ray diffraction analysis of cystathionine γ-synthase from *E. coli*, *FEBS Lett. 414*, 492−496.
27. Smith, D. R., Doucette-Stamm, L. A., Deloughery, C., Lee, H., Dubois, J., Aldredge, T., Bashirzadeh, R., Blakely, D., Cook, R., Gilbert, K., Harrison, D., Hoang, L., Keagle, P., Lumm, W., Pothier, B., Qiu, D., Spadafora, R., Vicaire, R., Wang, Y., Wierzbowski, J., Gibson, R., Jiwani, N., Caruso, A., Bush, D., Reeve, J. N., et al. (1997) Complete genome sequence of *Methanobacterium thermoautotrophicum* ΔH: Functional analysis and comparative genomics, *J. Bacteriol. 179*, 7135−7155.
28. Slesarev, A. I., Mezhevaya, K. V., Makarova, K. S., Polushin, N. N., Shcherbinina, O. V., Shakhova, V. V., Belova, G. I., Aravind, L., Natale, D. A., Rogozin, I. B., Tatusov, R. L., Wolf, Y. I., Stetter, K. O., Malykh, A. G., Koonin, E. V., and Kozyavkin, S. A. (2002) The complete genome of hyperthermophile *Methanopyrus kandleri* AV19 and monophyly of archaeal methanogens, *Proc. Natl. Acad. Sci. U.S.A. 99*, 4644−4649.
29. Hendrickson, E. L., Kaul, R., Zhou, Y., Bovee, D., Chapman, P., Chung, J., Conway de Macario, E., Dodsworth, J. A., Gillett, W., Graham, D. E., Hackett, M., Haydock, A. K., Kang, A., Land, M. L., Levy, R., Lie, T. J., Major, T. A., Moore, B. C., Porat, I., Palmeiri, A., Rouse, G., Saenphimmachak, C., Soll, D., Van Dien, S., Wang, T., Whitman, W. B., Xia, Q., Zhang, Y., Larimer, F. W., Olson, M. V., and Leigh, J. A. (2004) Complete genome sequence of the genetically tractable hydrogenotrophic methanogen *Methanococcus maripaludis*, *J. Bacteriol. 186*, 6956−6969.
30. Hall, B. G., Yokoyama, S., and Calhoun, D. H. (1983) Role of cryptic genes in microbial evolution, *Mol. Biol. Evol. 1*, 109−124.
31. Li, W. H. (1984) Retention of cryptic genes in microbial populations, *Mol. Biol. Evol. 1*, 213−219.
32. Forchhammer, K., and Böck, A. (1991) Selenocysteine synthase from *Escherichia coli*. Analysis of the reaction sequence, *J. Biol. Chem. 266*, 6324−6328.
33. Engelhardt, H., Forchhammer, K., Müller, S., Goldie, K. N., and Böck, A. (1992) Structure of selenocysteine synthase from *Escherichia coli* and location of tRNA in the seryl-tRNA(Sec)-enzyme complex, *Mol. Microbiol. 6*, 3461−3467.
34. Fujii, T., Maeda, M., Mihara, H., Kurihara, T., Esaki, N., and Hata, Y. (2000) Structure of a NifS homologue: X-ray structure analysis of CsdB, an *Escherichia coli* counterpart of mammalian selenocysteine lyase, *Biochemistry 39*, 1263−1273.
35. Kaiser, J. T., Clausen, T., Bourenkow, G. P., Bartunik, H. D., Steinbacher, S., and Huber, R. (2000) Crystal structure of a NifS-

like protein from *Thermotoga maritima*: Implications for iron sulphur cluster assembly, *J. Mol. Biol. 297*, 451−464.
36. Clausen, T., Kaiser, J. T., Steegborn, C., Huber, R., and Kessler, D. (2000) Crystal structure of the cystine C-S lyase from *Synechocystis*: Stabilization of cysteine persulfide for FeS cluster biosynthesis, *Proc. Natl. Acad. Sci. U.S.A. 97*, 3856−3861.
37. Jansonius, J. N. (1998) Structure, evolution and action of vitamin B6-dependent enzymes, *Curr. Opin. Struct. Biol. 8*, 759−769.
38. Zheng, L., White, R. H., Cash, V. L., and Dean, D. R. (1994) Mechanism for the desulfurization of L-cysteine catalyzed by the nifS gene product, *Biochemistry 33*, 4714−4720.
39. Clausen, T., Huber, R., Prade, L., Wahl, M. C., and Messerschmidt, A. (1998) Crystal structure of *Escherichia coli* cystathionine γ-synthase at 1.5 angstrom resolution, *EMBO J. 17*, 6827−6838.
40. Tormay, P., Wilting, R., Heider, J., and Böck, A. (1994) Genes coding for the selenocysteine-inserting tRNA species from *Desulfomicrobium baculatum* and *Clostridium thermoaceticum*: Structural and evolutionary implications, *J. Bacteriol. 176*, 1268−1274.
41. Sauerwald, A., Zhu, W., Major, T. A., Roy, H., Palioura, S., Jahn, D., Whitman, W. B., Yates, J. R., III, Ibba, M., and Söll, D. (2005) RNA-dependent cysteine biosynthesis in archaea, *Science 307*, 1969−1972.
42. Copeland, P. R., Fletcher, J. E., Carlson, B. A., Hatfield, D. L., and Driscoll, D. M. (2000) A novel RNA binding protein, SBP2, is required for the translation of mammalian selenoprotein mRNAs, *EMBO J. 19*, 306−314.

BI051110R